J Supercond Nov Magn (2012) 25:2003–2008
DOI 10.1007/s10948-012-1548-7

ORIGINAL PAPER

Synthesis and Characterization of PEG-Sr Hexaferrite by Sol–Gel Conversion

A. Baykal · Z. Durmus · M.S. Toprak · H. Sozeri

Received: 28 January 2012 / Accepted: 26 March 2012 / Published online: 17 April 2012

Abstract Sr-M-type hexagonal ferrites have been prepared via a sol–gel route, and the effects of addition of different molecular weight polyethylene glycol (PEG) into the sol solutions on the static magnetic properties and particle morphology have been studied. Crystalline phases of the samples were determined by XRD analysis. FT-IR and TG analyses were used to prove the presence of PEG on $SrFe_{12}O_{19}$. The results showed that adding PEG with different molecular weight into the sol solutions affected the formation mechanism of $SrFe_{12}O_{19}$. Sr-M precursors prepared by various PEG types show different magnetic behaviors after precalcination at 150 °C. This discrepancy is explained by the formation of a different phase during the synthesis of SrM particles.

Keywords Polyethylene glycol · Hexaferrites · Magnetization · SEM · XRD

1 Introduction

M-type hexaferrites having the general formula $MeFe_{12}O_{19}$, where Me = Ba, Sr, Pb with magnetoplumbite structure have extensive applications as promising materials for permanent magnets, high density recording media, telecommunication, magneto-optical and microwave devices, silent rooms, radar systems and military applications [1, 2]. The M-type hexagonal structure has five distinct Fe crystallographic sites, namely three octahedral (2a, 12k and 4f2), one tetrahedral (4f1) and one trigonal bipyramid (2b) [3]. Its magnetic and electrical properties should be modulated with preparation, composition and the distribution of the substituted cations at the five crystallographic sites.

Large number of synthetic techniques have been developed to control the particle size, shape and the properties of the materials [4–9]. It is difficult to obtain ultrafine and monodispersed particles by the commercial ceramic method (solid-state reaction) which involves the firing of stoichiometric mixture of barium carbonate and iron oxide at high temperatures (about 1200 °C) followed by milling to break up the aggregates [10]. In order to prepare highly homogeneous ultrafine particles of barium hexaferrite, several non-conventional low-temperature chemical methods were developed for the formation of ultrafine $BaFe_{12}O_{19}$ particles in last few years. These methods employed co-precipitation [11–14], hydrothermal [15–17], sol–gel [18–21], microemulsion [22], citrate precursor [23], salt melt method [24], glass crystallization [25, 26], sonochemical [27], combustion [28] and mechano-chemical activation [29, 30]. The chemical co-precipitation method is a low-cost technique compared to the other mentioned methods, suitable for mass production. The main drawback is that the particle size is not small and monodispersed enough for applications like recording media applications.

M-type strontium hexaferrite ($SrFe_{12}O_{19}$) was prepared firstly in the 1950s by Philips Laboratories [31]. Due to appropriate magnetic properties, chemical stability, and low cost compared with rare-earth compounds, it has attracted

A. Baykal (✉) · Z. Durmus
Department of Chemistry, Fatih University, B. Cekmece, 34500 Istanbul, Turkey
e-mail: hbaykal@fatih.edu.tr

M.S. Toprak
Functional Materials Division, Royal Institute of Technology (KTH), SE16440 Stockholm, Sweden

H. Sozeri
TUBITAK-UME, National Metrology Institute, P.O. Box 54, Gebze 41700, Kocaeli, Turkey

extensive interest in the past decades [32–34]. It is a hard magnet with high coercivity, which originates from high magnetocrystalline anisotropy with single easy magnetization axis. It has been recognized that it can be used as permanent magnets, recording media, telecommunication, and as components in microwave, higher-frequency, and magneto-optical devices [35–41].

Especially, the synthesis of strontium hexaferrite via the sol–gel technique is the focus of the present study due to the advantages of inexpensive precursors, a simple process, time saving and the resulting nano-sized powder.

2 Experimental

2.1 Instrumentation

X-ray powder diffraction (XRD) analysis was conducted on a Rigaku Smart Lab operated at 40 kV and 35 mA using CuK_α radiation ($\lambda = 1.54059$ Å).

Fourier transform infrared (FT-IR) spectra of the samples were recorded with a Perkin Elmer BX FT-IR infrared spectrometer in the range of 4000–400 cm^{-1}.

Scanning Electron Microscopy (SEM) analysis was performed, in order to investigate the microstructure of the samples, using Field Emission Gun JEOL 6335 F. The samples were coated with gold at 10 mA for 2 min prior to SEM analysis.

The thermal stability was determined by thermogravimetric analysis (TGA, Perkin Elmer Instruments model, STA 6000). The TGA thermograms were recorded for 5 mg of powder sample at a heating rate of 10 °C/min in the temperature range of 30–750 °C under nitrogen atmosphere.

VSM measurements were performed by using a Vibrating sample magnetometer (LDJ Electronics Inc., Model 9600) and magnetization measurements were carried out in an external field up to 15 kOe at room temperature.

2.2 Procedure

The starting materials, iron (III) nitrate nonahydrate ($Fe(NO_3)_3{\cdot}9H_2O$), strontium nitrate ($Sr(NO_3)_2$), sodium hydroxide (NaOH), citric acid ($C_6H_8O_7{\cdot}H_2O$), and PEG (polyethylene glycol) purchased from Merck, all were of analytical purity. Stoichiometric amounts of $Fe(NO_3)_3{\cdot}9H_2O$ and $Sr(NO_3)_2$ were dissolved in a small amount of deionized H_2O by stirring at 50 °C with Fe/Sr ratio of 12:1. Citric acid was then added to the mixture solution of Sr^{2+} and Fe^{3+} to chelate these ions. The molar ratios of citric acid to metal ions used were 1:1. Ammonia was added to adjust the pH value to 7. The solution was then divided into three parts. Then 2 g PEG (400, 2000, 10.000) was slowly added separately to the each solution and stirred magnetically at 65 °C for 2 h. Then PEG containing metal-citrate solutions were slowly evaporated at 80 °C under constant stirring until a viscous gel was formed. By increasing the temperature up to 150 °C, the gel precursors were combusted to form brown loose powders. Then the obtained precursor powders were pre-heated at 450 °C for 4 h and calcined at 1100 °C for 2 h. The hexaferrite nanoparticles were thus obtained.

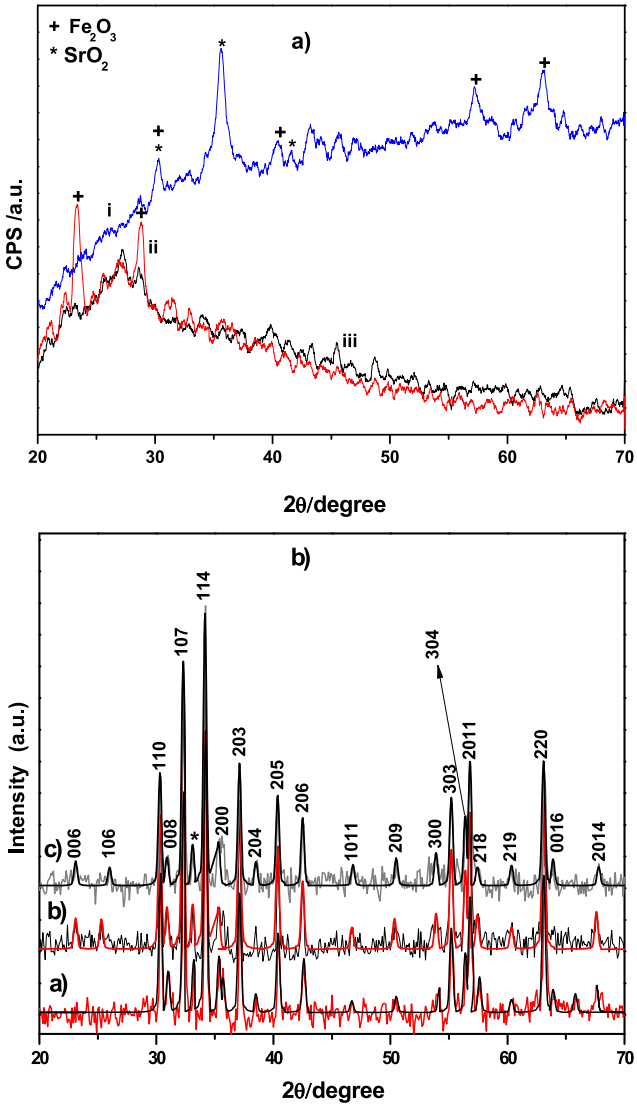

Fig. 1 (**a**) XRD powder pattern of precursor powders of (*i*) SrM-PEG 400, (*ii*) SrM-PEG 2000 and (*iii*) SrM-PEG 10.000 and (**b**) XRD powder pattern and line profile fitting of calcined powder of (*a*) SrM-PEG 400, (*b*) SrM-PEG 2000 and SrM-PEG (*c*) 10.000 after calcination at 1100 °C for 2 h

3 Results and Discussion

3.1 XRD Analysis

Phase investigation of precursors (heated at 150 °C) and the crystallized calcinated products of SrM-PEG 400, SrM-PEG

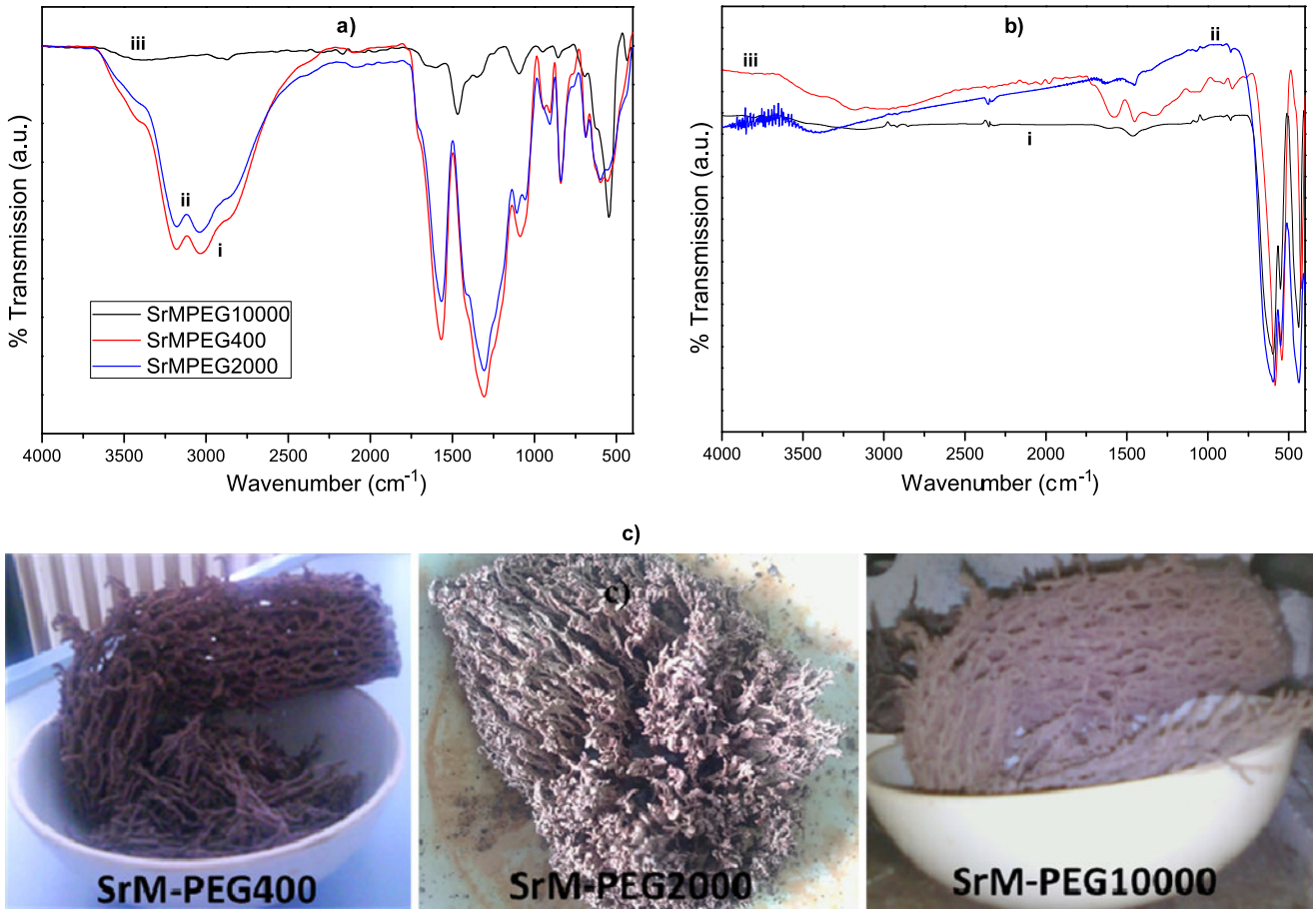

Fig. 2 FTIR spectra of (**a**) precursor powders of (*i*) SrM-PEG 400, (*ii*) SrM-PEG 2000 and (*iii*) SrM-PEG 10.000; (**b**) calcined powder of (*i*) SrM-PEG 400, (*ii*) SrM-PEG 2000 and (*iii*) SrM-PEG 10.000 at 1100 °C, and (**c**) photograph of the obtained powder of dendritic shape of SrM-PEG 400, SrM-PEG 2000 and SrM-PEG 10.000, respectively, after pre-heating at 450 °C for 4 h

2000 and SrM-PEG 10.000 were performed by XRD and the diffraction patterns were presented in Fig. 1a and 1b, respectively. The XRD powder pattern of SrM-PEG 10.000 precursor (heated at 150 °C) is different from that of precursor of SrM-PEG 400 and SrM-PEG 2000 (Fig. 1a). In the XRD pattern of SrM-PEG 400, SrM-PEG 2000 precursors, there was no indication of formation ferrites, their XRD patterns were almost amorphous, however, SrM-PEG 10.000 precursor (which was attracted by magnet) XRD pattern exhibits different diffraction pattern which has lines indicating the presence of SrO_2 (ICDD Card No.: 43-1031) and gamma-Fe_2O_3 (ICDD Card No.: 39-1346). This suggests that the effect of PEG 10.000 on hexaferrite formation is completely different from that of PEG 400 and PEG 2000.

The XRD powder patterns of calcined powders indicate that the products are M-type $SrFe_{12}O_{19}$ and the diffraction peaks are broadened owing to very small crystallite size. All of the observed diffraction peaks are indexed, as presented, by the hexagonal structure of $SrFe_{12}O_{19}$ revealing a high phase purity of hexaferrite agreeing with those reported for Sr hexaferrite (JCPDS card number 84-1531) including minor phase Fe_2O_3 with ICDD card No.: 76-1821 [42, 43]. The mean size of the crystallites were estimated from the diffraction pattern by line profile fitting method using (1) given in Refs. [44, 45]. The line profiles, shown in Fig. 1 were fitted for observed 24 peaks for SrM-PEG 400, SrM-PEG 2000 and SrM-PEG 10.000 calcined samples with the following Miller indices: (002), (102), (006), (105), (106), (110), (008), (107), (114), (200), (108), (203), (205), (206), (118), (207), (1011), (213), (209), (300), (303), (304), (1112), (218), (1014), (220), (1114), (2014), and (311). The average crystallite, sizes, D and σ, were obtained as 31 ± 4, 29 ± 3, 28 ± 2 nm for SrM-PEG 400, SrM-PEG 2000 and SrM-PEG 10.000, respectively, as a result of this line profile fitting.

3.2 FT-IR Analysis

Figure 2a represents the FT-IR spectra of precursor powders of SrM-PEG 400, SrM-PEG 2000 and SrM-PEG 10.000 Sr hexaferrites. As is seen from Fig. 2a, the FT-IR spectrum of percursor of SrM-PEG 10.000 is also different from that

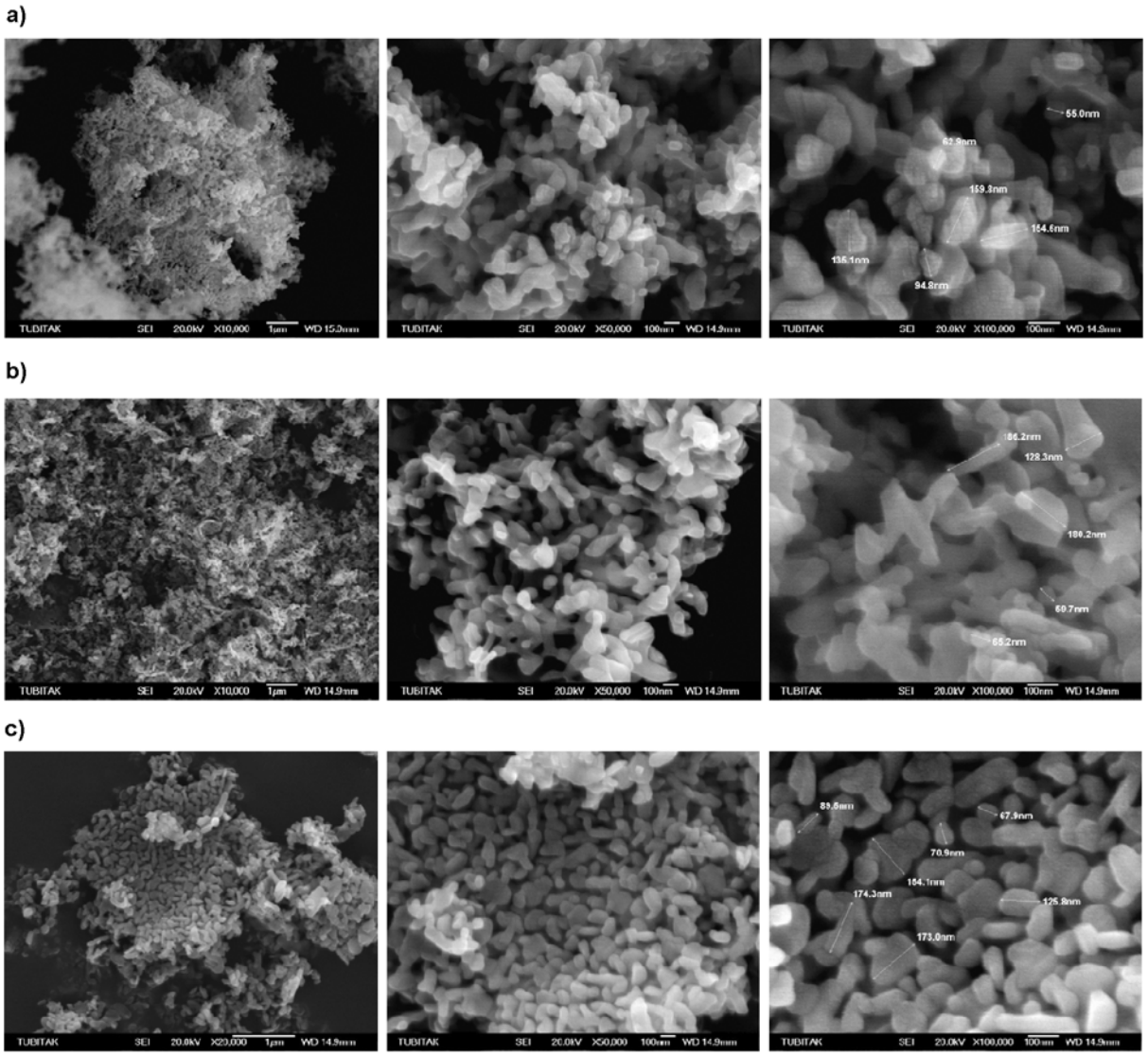

Fig. 3 SEM micrographs of calcined samples at 1100 °C of (**a**) SrM-PEG 400, (**b**) SrM-PEG 2000 and (**c**) SrM-PEG 10.000

of SrM-PEG 400, SrM-PEG 2000 precursors. In the FT-IR spectra of calcined samples of SrM-PEG 400, SrM-PEG 2000 and SrM-PEG 10.000. Figure 2b represents the calcined powder of SrM-PEG 400, SrM-PEG 2000 and SrM-PEG 10.000 at 1100 °C. Figure 2b presents characteristic peaks that are exhibited by the $SrFe_{12}O_{19}$ powder. The characteristic absorption bands for $SrFe_{12}O_{19}$ at around 591 and 438 cm^{-1} corresponding to vibrations of the tetrahedral and octahedral sites for $SrFe_{12}O_{19}$ in Fig. 2b [46, 47].

3.3 SEM Analysis

The morphology of calcined SrM-PEG 400, SrM-PEG 2000 and SrM-PEG 10.000 has been examined using SEM and Fig. 3 shows typical micrographs of samples under various magnifications. It is not possible to see the nanocrystallites—estimated from XRD analysis—via the SEM technique. Grains, sintered particles, exhibit polygonic morphologies and are aggregated. Grain size ranges from ca. 50 nm up to 160 nm for all three samples, without showing a clear variation with respect to the molecular weight of the PEG used in the synthesis process. This is mostly due to the high temperature used for the calcination that has smoothened the possible variations in the microstructure due to PEG molecular weight.

3.4 TG Analysis

Thermal analysis was performed to study the thermal stability of SrM-PEG 400, SrM-PEG 2000 and SrM-PEG 10.000 and TGA thermograms are presented in Fig. 4. The loss in all samples is expected to be mainly due to the loss of

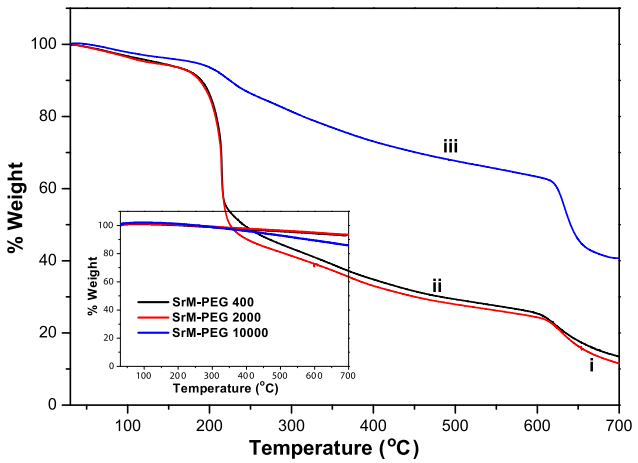

Fig. 4 TGA thermograms of precursor powder of SrM-PEG (*i*) 400, (*ii*) SrM-PEG 2000 and (*iii*) SrM-PEG 10.000 and the inset shows TGA thermograms of calcined powder samples

PEG polymer and therefore to be around the same extent. Thermograms for SrM-PEG 400, SrM-PEG 2000 show loss of adsorbed and crystalline water up to 180 °C at which the decomposition of the PEG species start, resulting in an overall loss of ca. 90 %. The thermogram for sample SrM-PEG 10.000, however, shows a similar trend with much less weight loss, ca. 60 %, in the investigated temperature range. This sample has also exhibited different characteristics in XRD as well as FTIR analyses. The observed difference is suggested to stem from the during the pre-heating phase at 150 °C part of the organic component may have combusted, thus leaving a smaller quantity of the PEG phase decomposing in the TGA analysis for SrM-PEG 10.000 precursor.

3.5 VSM Analysis

Figure 5 shows room temperature magnetization curves of SrM precursors and calcinated powders in the field range of ±15 kOe. After initial calcinations at 150 °C, precursors prepared by PEG 400 and 2000 have similar magnetic behavior in such a way that both have no coercivity and weak magnetization (around 0.1 emu/g) with no saturation. They behave like paramagnetic particles. On the other hand, SrM-PEG 10.000 precursor has small coercivity (≈200 Oe) and strong magnetization (>10 emu/g) in the same field range resembling a weak ferro- or ferrimagnetic behavior. Two different magnetic behaviors of the precursors of Sr hexaferrites can be explained by formation of different phases during pre-calcination at 150 °C. XRD patterns taken after this stage, in Fig. 1a, clearly reveal that SrM-PEG 1000 has a different phase compared to the other two samples. The peak at $2\theta = 33.50$ corresponds to SrO_2 phase which was not observed in the other precursors. After the calcinations at high temperatures, hard SrM phase

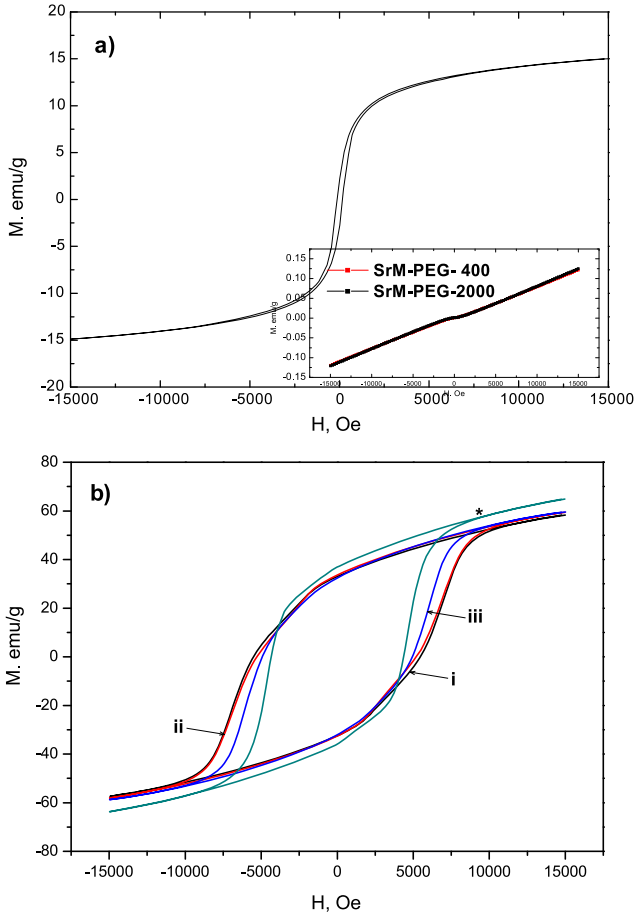

Fig. 5 M–H hysteresis curve of (**a**) SrM-PEG 10.000 precursor. *Inset* shows precursor powder of SrM-PEG 400 and SrM-PEG 2000; (**b**) (∗) Pure SrM and calcined powders of (*i*) SrM-PEG 400, (*ii*) SrM-PEG 2000 and (*iii*) SrM-PEG 10.000 at room temperature

is formed in all samples as shown in Fig. 5b. Sr hexaferrite prepared by different PEG types has approximately the same saturation magnetization around 60 emu/g and coercivity of 5.5 kOe. But the addition of PEG, even if they have different molecular weights, tune the magnetic properties of the M-type hexagonal ferrites. The same result was also observed by Han et al. [43].

4 Conclusion

M-type hexagonal ferrites ($SrFe_{12}O_{19}$) have been prepared via sol–gel synthesis technique using PEG 400, PEG 2000 and PEG 10.000, and magnetic properties and the crystalline phases of both precursors and calcinated products have been compared. Room temperature magnetization measurements of pre-calcinated SrM precursors prepared with different PEG inclusions showed different magnetic behavior. PEG 400 and 2000 included powders, for example, have paramagnetic-like magnetization while magnetization

of PEG 10.000 sample resembles soft ferro- or ferrimagnetic behavior with small coercive field. It was realized that $Sr_3Fe_2O_6$ phase starts to form after pre-calcination at 150 °C and observed discrepancy in M–H hysteresis curves probably due to this phase. Our results indicate that the addition of PEG with different molecular weights into the sol solution of can be an effective way to tune the magnetic properties of SrM (hexaferrites).

Acknowledgements The authors are thankful to the Fatih University, Research Project Foundation (Contract No.: P50021104-B and P50021104-G).

References

1. Hernandez, P., Francisco, C.D., Munoz, J.M., Iniguez, J., Torres, L., Zazo, M.: J. Magn. Magn. Mater. **157–158**, 123 (1996)
2. Jin, Z., Tang, W., Zhang, J., Lin, H., Du, Y.: J. Magn. Magn. Mater. **182**, 231 (1998)
3. Lechevallier, L., Breton, J.M.L., Wang, J.F., Harris, I.R.: J. Magn. Magn. Mater. **269**, 192 (2004)
4. Deligoz, H., Baykal, A., Tanrıverdi, E.E., Durmus, Z., Toprak, M.S.: Mater. Res. Bull. **47**, 537 (2012)
5. Ataie, A., Harris, I., Ponton, C.B.: J. Mater. Sci. **30**, 1429 (1995)
6. Fang, J., Wang, J., Gan, L.M., Ng, S.C., Ding, J., Liu, X.: J. Am. Ceram. Soc. **83**, 1049 (2000)
7. Iqbal, M.J., Ashiq, M.N.: Chem. Eng. J. **136**, 383 (2008)
8. Rezlescu, L., Rezlescu, E., Popa, P.D., Rezlescu, N.: J. Magn. Magn. Mater. **193**, 288 (1999)
9. Zhong, W., Ding, W., Zhang, N., Hong, J., Yan, Q., Du, Y.: J. Magn. Magn. Mater. **168**, 196 (1997)
10. Cabanas, M.V., González-Calbet, J.M.: Solid State Ionics **63–65**, 207 (1993)
11. Jacobo, S.E., Civale, L., Domingo-Pascual, C., Rodrigues-Clements, R., Blesa, M.A.: J. Mater. Sci. **32**, 1025 (1997)
12. Carp, O., Barjega, R., Segal, E., Brezeanu, M.: Thermochim. Acta **318**, 57 (1998)
13. Ogasawara, T., Oliveira, M.A.S.: J. Magn. Magn. Mater. **217**, 147 (2000)
14. Matutes-Aquino, J., Díaz-Castañón, S., Mirabal-García, M., Palomares-Sánchez, S.A.: Scr. Mater. **42**, 295 (1999/2000)
15. Wang, M.L., Shih, Z.W., Lin, C.-H.: J. Cryst. Growth **130**, 153 (1993)
16. Liu, X., Wang, J., Gan, L.-M., Ng, S.-C.: J. Magn. Magn. Mater. **195**, 452 (1999)
17. Mishra, D., Anand, S., Panda, R.K., Das, R.P.: Mater. Chem. Phys. **86**, 132 (2004)
18. Surig, C., Hempel, K.A., Sauer, Ch.: J. Magn. Magn. Mater. **157–158**, 268 (1996)
19. Zhong, W., Ding, W., Zhang, N., Hong, J., Yan, Q., Du, Y.: J. Magn. Magn. Mater. **168**, 196 (1997)
20. Garcia, R.M., Ruiz, E.R., Rams, E.E., Sanchez, R.M.: J. Magn. Magn. Mater. **223**, 133 (2001)
21. Mali, A., Ataie, A.: Scr. Mater. **53**, 1065–1070 (2005)
22. Palla, B.J., Shah, D.O., Garcia-Casillas, P., Matutes-Aquino, J.: J. Nanopart. Res. **1**, 215–221 (1999)
23. Sankaranarayanan, V.K., Khan, D.C.: J. Magn. Magn. Mater. **153**, 337 (1996)
24. Chin, T.S., Hsu, S.L., Deng, M.C.: J. Magn. Magn. Mater. **120**, 64–68 (1993)
25. El-Hilo, M., Pfeiffer, H., O'Grady, K., Schüppel, W., Sinn, E., Görnert, P., Rösler, M., Dickson, D.P.E., Chantrell, R.W.: J. Magn. Magn. Mater. **129**, 339 (1994)
26. Lee, C.K., Berta, Y., Speyer, R.F.: J. Am. Ceram. Soc. **79**, 183–192 (1996)
27. Shafi, K.V.P.M., Gedanken, A.: Nanostruct. Mater. **12**, 29 (1999)
28. Castro, S., Gayoso, M., Rivas, J., Greneche, J.M., Mira, J., Rodrigues, C.: J. Magn. Magn. Mater. **152**, 61–69 (1996)
29. Abe, O., Narita, M.: Solid State Ionics **101–103**, 103 (1997)
30. Gonzales-Angeles, A., Mendoza-Suarez, G., Gruskova, A., Toth, I., Jancarik, V., Papanova, M., Escalante-Garcia, J.I.: J. Magn. Magn. Mater. **270**, 77–83 (2004)
31. Went, J.J., Ratheneau, G.W., Gorter, E.W., VanDosterhout, G.W.: Philips Tech. Rev. **13**, 194 (1951)
32. Shirk, B.T., Buessem, W.R.: J. Appl. Phys. **40**, 1294 (1969)
33. Rensen, J.G., van Wieringen, J.S.: Solid State Commun. **7**, 113 (1969)
34. Kreber, E., Gonser, U., Trautwein, A., Harris, F.E.: J. Phys. Chem. Solids **36**, 263 (1975)
35. Coey, J.M.D.: J. Alloys Compd. **326**, 2 (2001)
36. Kazin, P.E., Trusov, L.A., Zaitsev, D.D., Tretyakov, Yu.D., Jansen, M.: J. Magn. Magn. Mater. **320**, 1068 (2008)
37. Morisako, A., Naka, T., Ito, K., Takizawa, A., Matsumoto, M., Hong, K.Y.: J. Magn. Magn. Mater. **242**, 304 (2002)
38. Hernandez, P., Francisco, C.D., Munoz, J.M., Iniguez, J., Torres, L., Zazo, M.: J. Magn. Magn. Mater. **157**, 123 (1996)
39. Jin, Z., Tang, W., Zhang, J., Lin, H., Du, Y.: J. Magn. Magn. Mater. **182**, 231 (1998)
40. Iqbal, M.J., Ashiq, M.N., Gomez, P.H., Munoz, J.M.: J. Magn. Magn. Mater. **320**, 881 (2008)
41. Shirk, B.T., Buessem, W.R.: J. Am. Ceram. Soc. **53**, 192 (1970)
42. Mou, F., Guan, J., Sun, Z., Fan, X., Tong, G.: J. Solid State Chem. **183**, 736 (2010)
43. Han, M., Ou, Y., Chen, W., Deng, L.: J. Alloys Compd. **474**, 185 (2009)
44. Wejrzanowski, T., Pielaszek, R., Opaliniska, A., Matysiak, H., Lojkowski, W., Kurzydlowski, K.J.: Appl. Surf. Sci. **253**, 204 (2006)
45. Pielaszek, R.: Analytical expression for diffraction line profile for polydispersive powders. In: Appl. Crystallography Proceedings of the XIX Conference, Krakow, Poland, vol. 43 (2003)
46. Gonzalez-Carreño, T., Morales, M.P., Serna, C.J.: Mater. Lett. **43**, 97 (2000)
47. Durmus, Z., Unal, B., Toprak, M.S., Sozeri, H., Baykal, A.: Polyhedron **30**, 1349 (2011)